Scripta Materialia 157 (2018) 129–134

Contents lists available at ScienceDirect

Scripta Materialia

journal homepage: www.elsevier.com/locate/scriptamat

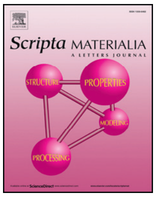

Regular article

Suppression of the lattice thermal conductivity in NbFeSb-based half-Heusler thermoelectric materials through high entropy effects

Jianlong Yan [a], Fusheng Liu [a,*], Guohua Ma [b], Bo Gong [a], Jiaxu Zhu [a], Xiao Wang [a], Weiqin Ao [a], Chaohua Zhang [a], Yu Li [a], Junqin Li [a]

[a] College of Materials Science and Engineering, Shenzhen University and Shenzhen Key Laboratory of Special Functional Materials, Shenzhen 518060, PR China
[b] Southwest University of Science and Technology, Mianyang, Sichuan 621010, PR China

ARTICLE INFO

Article history:
Received 27 June 2018
Received in revised form 26 July 2018
Accepted 7 August 2018
Available online xxxx

Keywords:
Spark plasma sintering
Thermoelectric materials
Thermal conductivity

ABSTRACT

$Nb_{1-x}M_xFeSb$ (M = Hf, Zr, Mo, V, Ti; equimolar) thermoelectric materials were prepared by arc melting and subsequent spark plasma sintering. NbFeSb-based half-Heusler phases with a high-entropy lattice were obtained by replacing the Nb sites with multielement M atoms. The lattice thermal conductivity decreased as the M content increased, which mainly resulted from the high entropy effect. A low lattice thermal conductivity of 2.5 W/m K and a high figure of merit of 0.88 were obtained at 873 K, showing the great promise of the high entropy strategy for reducing the lattice thermal conductivity and enhancing the thermoelectric performance.

Solid-state thermoelectric (TE) conversion achieved by the direct transformation of heat energy into electricity has tremendous promise for application in waste heat recycling. The conversion efficiency of a TE material is usually determined by a dimensionless figure of merit $ZT = S^2\sigma T/\kappa$, where S, T, σ and κ are the Seebeck coefficient, absolute temperature, electrical conductivity and thermal conductivity, respectively. κ can be divided into two parts, $\kappa = \kappa_l + \kappa_e$, where κ_l is the lattice thermal conductivity and κ_e is the carrier thermal conductivity. The power factor (PF, $=S^2\sigma$) is used to assess the electrical transport performance of a TE material. Approaches like maximizing the *PF* through optimal doping and band engineering [1–4] and reducing κ_l by nanostructural engineering [2,5–8] have been proposed to improve the TE performance. Among the various TE materials, half-Heusler (HH) compounds have recently gained considerable attention as promising materials for TE applications [9–12] because of their superior advantage of a high *PF* [13] and high thermal and mechanical stabilities [1,2,14,15]. Furthermore, these HH compounds are made of earth-abundant elements that are environmentally friendly and economical for wide-spread use [16].

ABX-type HH compounds possess a space group of *F*-43*m*, where A, B, and X in ABX represent an electropositive transition metal (commonly Ti, Zr, Nb or Hf) at the 4b (1/2, 1/2, 1/2) site, a transition metal (e.g., Co, Fe or Ni) at the 4c (1/4, 1/4, 1/4) site and a main-group *sp*-hybridized element (either Sn or Sb) at the 4a (0, 0, 0) site respectively. The covalent hybridization of the A and X atoms in the ABX compounds is calculated to be the key interaction responsible for the formation of so-called d–d gap in these compounds with a valence electron count of 18 separating the bonding states from the antibonding states, whose electronic density of states is favourable for achieving a large Seebeck coefficient and good electrical conductivity [6]. The presence of the *sp*-hybridized element X is also crucial because it not only hybridizes with A and B but also provides a channel to accommodate extra *d* electrons to stabilize these systems [17].

Considerable research efforts on p- [14,18] and n-type ABX HHs [19,20], which are mostly based on MCoSb, MNiSn, MFeSb (where M is Ti, Zr, Nb, or Hf), NbCoSn [21–25] and VFeSb [26], have been reported recently. HH compounds usually have high electrical conductivities and high Seebeck coefficients, yielding a high PF [2,6,15,27]. However, reducing the high κ_l is still the largest challenge for achieving a high TE performance in HH compounds [28]. The κ_l values of HH compounds based on MCoSb (M = Ti, Zr or Hf) have been reported to be 10–20 W/m K at room temperature and 8–15 W/m K at 500 °C [16,29,30]. The high substitutability of the three lattice sites (A, B, and X) provides many possibilities for tuning the electronic and thermal conductivities of HHs. Moreover, doping the HH compounds can also introduce various point defects, mass fluctuations and strain fields, which can be utilized to effectively scatter short- and mid-wavelength heat-carrying phonons to reduce κ_l [31]. The maximum ZT value of NbFeSb was found to reach 1.1 at 1000 K by doping 20% Ti at the Nb site [11,18]. When Hf is doped in the Nb site, the ZT value of $FeNb_{0.88}Hf_{0.12}Sb$ reaches a maximum of 1.5 at 1200 K [32].

High-entropy alloys have an enhanced configurational entropic contribution and can thermodynamically stabilize the formation of solid

---

[*] Corresponding author.
E-mail address: fsliu@szu.edu.cn (F. Liu).

https://doi.org/10.1016/j.scriptamat.2018.08.008
1359-6462/

solutions [33,34]. In high-entropy alloys, all of the phonon scattering strategies can in principle be achieved simultaneously through the intrinsically complex nature of these materials [15,27,34]. High-entropy alloys offer a large degree of complexity through severe lattice distortion, numerous point defects, and precipitation of secondary phases to scatter phonons effectively [34]. If several different elements were introduced into one of the sublattice of HHs such as 4a, 4b and 4c, the corresponding sublattice can be regarded as a high-entropy sublattice. Thus, the high entropy effect in HH compounds is proposed to have a substantial effect on reducing κ_l.

Here, we report a high entropy strategy for reducing the κ_l of NbFeSb-based HH compounds. A series of $Nb_{1-x}M_xFeSb$ (M = Ti, V, Hf, Mo, or Zr with an equimolar ratio) HH compounds are prepared, and the maximum *PF* of these samples reaches 6500 μW/m K^2 at 473 K. Moreover, the κ and κ_l values of NbFeSb both drastically decrease. The minimum κ_l of 2.5 W/m/K is obtained for $Nb_{0.6}M_{0.4}FeSb$ at 873 K, and a large ZT value of 0.88 is achieved for $Nb_{0.8}M_{0.2}FeSb$ at 873 K.

Elemental metals Hf (99.9%), Mo (99.9%), Nb (99.9%), Ti (99.9%), V (99.9%), Zr (99.9%), Fe (99.9%), and Sb (99.9%) were used to synthesize $Nb_{1-x}M_xFeSb$ (M = Ti, V, Hf, Mo, Zr) samples, where M is a mixture of the five elements Ti, V, Hf, Mo and Zr in an equimolar ratio. The weight loss due to the high vapour pressure of Sb was compensated for by the addition of 5% Sb. All samples were prepared by arc melting in three or more cycles under a pure argon atmosphere. Then, the as-cast ingots were sealed in a fused-silica tube under a pressure of 10^{-3} Pa, heated to 1100 °C, held at that temperature for a week, and then finally quenched in cold water. The final samples were sintered by spark plasma sintering (SPS) at 900 °C for 6 min under an axial pressure of 50 MPa. All electrical and thermal transport measurements were conducted in the temperature range from 300 to 823 K.

X-ray powder diffraction (XRD) experiments were conducted on a D8 Advance SS/18KW (Bruker, Germany) diffractometer equipped with a Cu Kα radiation source to analyse the phases of the samples. The Seebeck coefficient (S) and electrical resistivity (ρ, $1/\sigma$) were measured by a ZEM-2 instrument (Ulvac-Riko, Japan). The thermal conductivity (κ) was measured according to the formula $\kappa = \lambda\, C_p\, d$, where λ is the thermal diffusivity, C_p is the heat capacity, and d is the sample density. λ and C_p were measured by a laser flash technique using a TC-9000H thermal constant measuring system (Ulvac-Riko, Japan). The microstructures of the samples were observed by scanning electron microscopy (SEM) using a Hitachi SU-70 instrument coupled with energy-dispersive X-ray spectroscopy (EDS). The room temperature carrier concentration was tested by a physical properties measurement system (PPMS-9, Quantum Design).

Fig. 1 shows the XRD patterns of the samples in which the NbFeSb-based HH phase can be identified. The observation of several very weak peaks between the angles of 29° and 43° indicates the presence of trace $ZrSb_2$ and $NbSb_2$ phases. As shown in the inset of Fig. 1, the lattice parameter a obtained by the Rietveld refinement method remains almost unchanged as the doping amount x increases. The value 5.952 (1)Å of the un-doped sample is very close to the value reported for NbFeSb [35]. The average covalent radius of M is 1.346 Å, which is almost equal to the Nb covalent radius of 1.34 Å. Representative SEM images of $Nb_{0.85}M_{0.15}FeSb$ and $Nb_{0.9}M_{0.1}FeSb$ are shown in Fig. 2. The images show three different areas. As confirmed by EDS analysis, the bright, darker and darkest areas belong to the $NbSb_2$ phase, HH1 phase and HH2 phase, respectively. The grain sizes of the regular HH phases are approximately 5–40 μm. The chemical compositions of the phases are listed in Table 1 and are consistent with the nominal composition. The results also indicate that Zr mainly exists in the $NbSb_2$ phase or $ZrSb_2$ phase, as the Zr doping level in the NbFeSb phase is far below the nominal level. The slightly brighter HH1 phase has a slightly higher doping content of the M elements than the HH2 phase. Elemental mapping of the samples shows that the doping elements are uniformly distributed in the HH compounds, indicating the homogenous doping of M atoms in the HH compounds (Supplementary materials, S1). As revealed in Table 1, the Vickers hardness (HV) of the $Nb_{1-x}M_xFeSb$ samples dramatically increases from 484 to 861 as the M doping content x increases from 0 to 0.1 but does not change much as the M doping content x continues to increase from 0.1 to 0.4. The improvement in the HV can be mainly ascribed to the solid-solution strengthening mechanism.

Reportedly, the electronic structure $NbSb_2$ has no energy gap with metallic electrical conductivity behaviour [36], the electrical resistivity is on the level of 10^{-6} Ω·m at room temperature, and $ZrSb_2$ also has metallic electrical conductivity behaviour with electrical resistivity on the level of 10^{-7} Ω·m at room temperature [37]. The weight percentages of $NbSb_2$ and $ZrSb_2$ are below 2 wt% with Rietveld refinement. The grain sizes of the two phases are mainly larger than 10 μm. Therefore, due to the low amounts and large grain sizes, the existence of the two impurities' phases may slightly benefit the increase in electrical conductivity, with no obvious benefit for reducing thermal conductivity. Precipitations will have a substantial effect on reducing the thermal conductivity only on the nanometre level; however, because the doping element Zr prefers to exist in the $NbSb_2$ phase or the $ZrSb_2$ phase, which will significantly weaken the doping effect of Zr, the doping of Zr to Nb will benefit the increase in electrical conductivity and the slight decrease in lattice thermal conductivity [38].

The temperature-dependent electrical resistivity, Seebeck coefficient and PF of the $Nb_{1-x}M_xFeSb$ samples are shown in Fig. 3. The electrical resistivity of the $Nb_{1-x}M_xFeSb$ HH alloys drastically decreases by approximately two orders of magnitude (from 10^{-4} to 10^{-6} Ω·m) with the addition of M atoms from $x = 0$ to 0.1 (Fig. 3a). The electrical resistivity of the un-doped sample is in accordance with the reported data [32]. The Pauling electronegativity of Nb (1.6) is larger than that of Ti (1.54), Hf (1.3) and Zr (1.33). As shown in Fig. 3a and b, the electrical resistivity decreases as the amount of M atoms in the Nb sites increases, which is mainly ascribed to the increase in the hole carrier concentration. For an intrinsic semiconductor with a low carrier concentration, the resistivity decreases with increasing temperature due to thermal excitation of the carriers. For a heavily doped semiconductor, the electric resistivity increases with the temperature, showing metallic conduction characteristics. As shown in Fig. 3a, the electrical resistivity shows intrinsic semiconductor behaviour with a $T^{-1.2}$ temperature dependence for the un-doped sample ($x = 0$) but metallic behaviour with a $T^{1.5}$–$T^{0.5}$ temperature dependence for the doped samples ($x =$ 0.1 to 0.4). The $T^{1.5}$ and $T^{0.5}$ temperature dependence of the resistivity is usually ascribed to the mechanisms of phonon scattering and alloy scattering, respectively. Thus, as the M doping content increases, the carrier scattering mechanism changes from phonon scattering to alloy scattering. As shown in Fig. 3b, the carrier concentration of the $Nb_{1-x}M_xFeSb$ samples increases from 1.07×10^{22} cm^{-3} for $x = 0.1$ to 2.91×10^{22} cm^{-3} for $x = 0.4$, and the corresponding carrier mobility decreases from 1.7 to 0.8 $cm^2\ V^{-1}\ s^{-1}$, which is mainly due to an increase in carrier scattering from the large amount of lattice distortion in the high-entropy alloys.

The Seebeck coefficient of $Nb_{1-x}M_xFeSb$ decreases with the increase in the M content below 773 K, as shown in Fig. 3c. The reduction in the Seebeck coefficient of the $Nb_{1-x}M_xFeSb$ samples along with the decrease in the electrical resistivity can be ascribed to an increase in the carrier concentration (Fig. 3b). Intrinsic thermal excitation, which leads to a decrease in S, is suppressed at high temperatures for the doped samples, which makes the S values of the samples with $x = 0.1$, 0.15, and 0.2 larger than that of the un-doped sample. The PF of the $Nb_{1-x}M_xFeSb$ samples is dramatically improved (Fig. 3d), reaching a maximum value of 6500 μW/m K^2 at 373 K for the sample with $x =$ 0.1, which is nearly the same as that reported for $Nb_{0.88}Hf_{0.12}FeSb$ at 900 K (6400 μW/m K^2) [32]. The maximum value for the doped samples is also much larger than the maximum value for the pure sample, which is only 500 μW/m K^2 at 673 K.